Case Studies in Thermal Engineering 14 (2019) 100505

Contents lists available at ScienceDirect

Case Studies in Thermal Engineering

journal homepage: www.elsevier.com/locate/csite

Understanding of temperature and cooling effectiveness sensitivity of a film-cooled vane under coolant inlet temperature effect: A case study

Prasert Prapamonthon[a,b], Bo Yin[a,*], Guowei Yang[a], Mohan Zhang[a,c]

[a] Key Laboratory for Mechanics in Fluid Solid Coupling Systems, Institute of Mechanics, Chinese Academy of Sciences, Beijing, 100190, China
[b] Department of Aeronautical Engineering, International Academy of Aviation Industry, King Mongkut's Institute of Technology Ladkrabang, Bangkok, 10520, Thailand
[c] School of Engineering Science, University of Chinese Academy of Sciences, Beijing, 100049, China

ARTICLE INFO

Keywords:
Cooling performance
Film cooling
Coolant inlet temperature
Surface temperature

ABSTRACT

This work presents a case study of the relationship between temperature and cooling effectiveness of a film-cooled vane under effect of coolant inlet temperature in two aspects based on the actual and base coolant inlet temperatures. Results are conducted in terms of temperature, cooling effectiveness, and heat transfer coefficient based on surface and volume analyses using CFD/CHT approach. Sensitivity of the vane temperature and cooling effectiveness under this effect is discussed also. The results show that for the surface basis, although the cooling effectiveness obtained from the actual coolant inlet temperature is quite straightforward and follows the definition of the cooling effectiveness directly, the cooling effectiveness obtained from the base coolant inlet temperature is more understandable because it corresponds to the variation of the surface temperature. Based on the volume basis and the base coolant inlet temperature, the 8% increase in the coolant inlet temperature causes the reduction of the average and maximum cooling effectiveness, which corresponds to 18 K and 25 K increments in the average and minimum temperatures, respectively. However, when the actual coolant inlet temperature is used, the variation of the cooling effectiveness is rather insensitive due to the reduction of heat flux on the hot-side wall.

1. Introduction

It is well-known that thermal efficiency and power output produced by a gas-turbine engine depend upon the turbine inlet temperature. Ideally, the gas-turbine engine needs to operate under high turbine inlet temperatures to reach high thermal efficiency and power output. Unfortunately, in reality, the allowable turbine inlet temperature is limited by the survivability of hot component materials, especially airfoils of the 1st stage nozzle guide vane of high-pressure gas turbines. Following the operation at high temperatures, the turbine airfoils suffer from thermal damage caused by heat transfer from high thermal loads, thereby reducing a lifespan of the airfoils. Therefore, the turbine airfoils need effective cooling systems to prolong hour service. Presently, turbine airfoils of a state-of-the-art gas turbine contain internal passages for coolant taken from the compressor. The cool air is used for internal cooling and external cooling, called film cooling, to reduce the metal temperature. The film cooling is used to protect the external surface which is under a complex flow field. These cause a variation of local heat transfer coefficient and local temperature on the

* Corresponding author.
E-mail address: yinbo@imech.ac.cn (B. Yin).

https://doi.org/10.1016/j.csite.2019.100505
Received 18 June 2019; Received in revised form 17 July 2019; Accepted 21 July 2019
Available online 23 July 2019

hot-side wall and also lead to a variation of the airfoil surface temperature, including temperature gradient due to heat conduction within the airfoil material. As described, heat convection from film cooling, internal cooling and heat conduction within the airfoil material are intrinsically linked, thereby making the overall thermal problem complicated and difficult. Therefore, it is important to understand the cooling performance of the turbine airfoils operating under the combined mode of heat transfer and fluid flow. Cooling effectiveness is an important parameter used to describe the cooling performance due to the fact that this parameter reflects on conductive heat within the vane material, including the thermodynamic temperature of the hot mainstream and coolant from the hot and cold sources. So far, thermal prediction on the cooling performance of turbine airfoils has been conducted by many researchers [1–7] using computational fluid dynamics (CFD) with conjugate heat transfer (CHT) analysis. Their results indicated that CFD/CHT analysis can provide acceptable results in the airfoil temperature and heat transfer coefficient obtained from problems of the three modes of heat transfer with fluid flow. Besides, several researchers also investigated the thermal sensitivity and the cooling effectiveness under effects of aerothermal uncertainties in boundary conditions, especially from the coolant passage. For examples, Reyhani et al. [5] studied sensitivity to coolant inlet pressure and temperature, including load variation to turbine blade temperature calculation and life estimation. Alizadeh et al. [6] studied uncertainties on parameters that affect heat transfer parameters of turbine blades such as turbine inlet temperature and pressure, and rotor coolant inlet pressure and temperature. Their results indicated that the uncertainty of these parameters has significant impacts on the blade temperature. Kim et al. [8] evaluated sensitivity to operating parameters on the predicted blade temperatures and stresses. Their results showed the spatially resolved sensitivity of the operating parameters on blade temperature and stress distributions. Williams et al. [9] conducted sensitivity of overall effectiveness to film cooling and internal cooling on the suction surface of a turbine vane. Their investigation showed that overall cooling effectiveness increases at higher momentum flux ratios obtained from adjusting the coolant flow rate. Espinosa et al. [10] evaluated the effect of cooling airflow rate reduction on the blade surface temperature distribution. Their results showed that the temperature distribution is related to the cooling effectiveness, on the coolant flow rate in the cooling passages. Roos [11] carried out sensitivity analyses of the trailing edge ejection slot width on cooling performance in a nozzle guide vane. His study indicated that the reduction in the slot size causes a corresponding decrease in the coolant mass flow rate, thereby increasing in the blade temperature. Nathan et al. [12] investigated the cooling effectiveness of a showerhead film-cooled vane under the effects of the momentum flux ratio. Their results showed that the cooling effectiveness increases as the momentum flux ratio increases.

Although there have been several studies of cooling performance of the turbine airfoils so far, the investigation of effects of the parameter uncertainties is still challenging, because overall thermal problems obtained from a turbine airfoil are complicated, as mentioned previously, especially if a vane is cooled by intricate cooling systems. This work aims to propose a case study of characteristics of the cooling effectiveness, which is commonly used for the cooling performance discussion of the turbine airfoils, under the effect of coolant inlet temperature constrained by the compressor supply in two aspects i.e. actual and base coolant inlet temperatures. A numerously film-cooled vane of the 1st stage nozzle guide vanes is used to carry out the vane temperature, cooling effectiveness, and heat transfer coefficient based on the analysis of the surface and volume bases by means of CFD/CHT approach. The sensitivity of the vane temperature and cooling effectiveness under the effect of coolant inlet temperature is discussed also.

2. Vane model and numerical technique

In this work, the 1st stage high-pressure turbine vane reported by Halila et al. [13] is adopted. This vane consists of two coolant passages where are connected to 217 film holes from 13 rows for film cooling protection on the vane surface. In addition, a baffle with 131 and 216 impingement holes is inserted within the forward and real passages, respectively, for heat transfer enhancement.

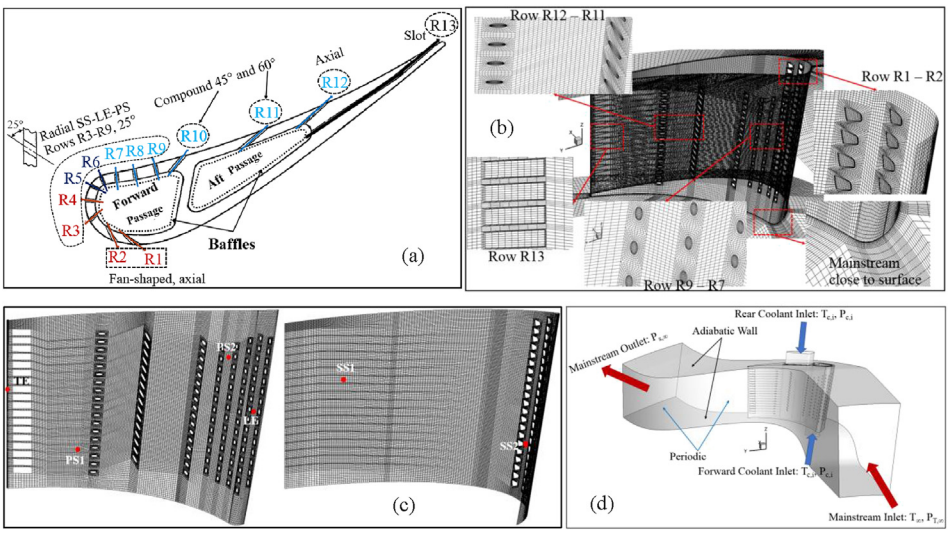

Fig. 1. (a) Configuration of film holes at midspan, (b) computational mesh, (c) location of six-point monitor and (d) boundary conditions.

All film hole rows are placed orderly, namely, R1 – R4 on the suction surface (SS), R5 – R6 on the leading edge (LE), R7 – R12 on the pressure surface (PS) and R13 on the PS close to the trailing edge (TE), as seen in Fig. 1(a). More details about the film holes can be seen in Halila et al. [13].

ANSYS ICEM is used to generate the mesh for the whole computational domain. The mesh is divided into fluid and solid domains. In the fluid domain, meshes are mainly H-type meshes and meshes close to the sold domain are stretched with 8–12 layers which suffice to resolve flow in the boundary layer. The computational mesh used in this work is the same as studied by Zhang et al. [14]. The mesh independence was approved by comparing the surface temperature at the midspan using three numbers of mesh elements i.e. 7, 11 and 16 million. It was found that the temperature distributions obtained by 11 and 16 million elements agreed well to each other with a maximum error of 2%, which is acceptable for engineering work. Therefore, the mesh with 11 million elements is used for all calculations. This mesh has the averaged Y^+ of about 5, which is acceptable for accurate simulation of flow in the boundary layer. Some parts of the mesh are depicted in Fig. 1(b).

ANSYS FLUENT is used as the solver and the SST k-ω turbulence model is employed because this turbulence model has shown accurate and acceptable results as previously presented by Refs. [1,2,5,7,15]. The heat transfer problem in the present work is solved by CFD/CHT approach, mesh interface technique is applied to all interfaces between the solid and fluid domains in order to obtain equivalent temperature at solid-fluid interfaces, thereby reaching accurate prediction of heat flux. For the convergence criteria of solutions, the continuity and energy residuals must be lower than 10^{-3} and 10^{-7}, respectively. Mass flow balance of all inlets and outlets is also checked to ensure the convergence of the solutions. In addition, six-point surface temperatures on the PS, LE, SS, and TE are monitored, as illustrated in Fig. 1(c). Following the convergence criteria, the six-point temperatures must keep unchanged with the subsequent iterations to confirm the convergence of the solutions.

For boundary conditions, the boundary conditions are set as reported by Timko [16] and main parts of the boundary conditions are shown in Fig. 1(d). The mainstream inlet is the hot air with a uniform total temperature and pressure of 709 K and 3.4474×10^5 Pa, respectively. The pressure ratio, which is the ratio between the total inlet pressure to the static outlet pressure of the mainstream, is set as 1.67. Air is also worked as a working fluid of the coolant, which is supplied by the two passages. The total temperature and pressure of the coolant at the inlet are uniformly set as 339 K and 3.5095×10^5 Pa, respectively. For other quantities, the mainstream turbulence intensity (Tu) is 10% and turbulence length scales (Lu) at the inlets and the outlet are the same values as previously studied by Zhang et al. [14]. Additionally, because the mainstream passage of the studied vane is designed as an annular cascade with a rotational angle of 7.826° in accordance with the design of 46 nozzle guide vanes, so the periodic boundary condition with the rotational angle of 7.826° is applied to relieve the limitation of time-consuming difficulty and computational cost. Following this condition, numerical results are still meaningful. All boundary conditions are given in Table 1.

For material properties, the vane material is made of steel and air is used for the mainstream and coolant. Thermal conductivity and specific heat capacity of steel and air are expressed linearly in terms of the temperature. The density of air is governed by the ideal gas law and its viscosity is computed by Sutherland Law. Table 2 lists all material properties used in the present work.

To obtain a better understanding of the cooling effectiveness and vane temperature, the variation of the coolant inlet temperature from the default value of 339 K is used as the studied independent variable for the cooling performance sensitivity. The studied range of the coolant inlet temperature is listed in Table 3.

3. Validation

The studied vane used in the present work has the same geometry and computational mesh as Zhang et al. [14] did before. The validation of numerical results obtained by SST k-w model was approved by Zhang et al. [14] in terms of Mach number (*Ma*) along the vane surface at the midspan. It was found that in general, the SST k-w model provides acceptable *Ma* when compared to the experimental data reported by Timko [16]. However, it should be noted that the heat transfer validation has not been approved yet due to lack of thermal experimental data from Timko [16], including other opened works of literature. Therefore, all results of the present work are conducted under the favorable assumption that the method which provides reasonable prediction in an aerodynamic agreement such as Mach number, pressure, and velocity distributions could give reasonable and acceptable prediction in the thermal field, as seen in previously published literature [1,2,5,7,15,18,19]. Therefore, the validation of aerodynamic results done by Zhang et al. [14] is still meaningful for heat transfer prediction and the solver with SST k-w model is used for the subsequent simulations.

Table 1
Boundary conditions [14,16].

Boundary	Condition
Mainstream inlet	T_∞ = 709 K, $P_{T,\infty}$ = 3.4474×10^5 Pa, Tu = 10%, Lu = 0.4 cm
Mainstream outlet	PR = 1.67, Lu = 0.305 cm
Forward coolant inlet	$T_{c,i}$ = 339 K, $P_{T,c,i}$ = 3.5095×10^5 Pa, Tu = 5%, Lu = 0.064 cm
Forward coolant outlet	Adiabatic wall with non-slip condition
Aft coolant inlet	$T_{c,i}$ = 339 K, $P_{T,c,i}$ = 3.5095×10^5 Pa, Tu = 5%, Lu = 0.038 cm
Aft coolant outlet	Adiabatic wall with non-slip condition

Table 2
Details of material properties [14,17].

Property	Steel	Air
Density (kg/m^3)	8055	Ideal gas
Thermal conductivity (W/m·K)	11.2 + 0.0144T	0.01019 + 0.000058T
Specific heat capacity (J/kg·K)	438.5 + 0.177T	938 + 0.196T
Viscosity (kg/m·s)	-	Sutherland Law

*T in Kelvin.

Table 3
Independent variable used as sensitivity parameter.

Parameter	Range of variation
Increment of coolant inlet temperature ($\Delta T_{c,i}$): Coolant forward passage	0–8%
Increment of coolant inlet temperature ($\Delta T_{c,i}$): Coolant aft passage	0–8%

4. Results and discussion

Numerical results are conducted in terms of heat transfer parameters i.e. the cooling effectiveness, temperature, and heat transfer coefficient under the variation of the coolant inlet temperature. At first, the results in Sections 4.1 and 4.2 are presented based on the vane surface basis. Then, the analysis based on the vane volume basis is described in Section 4.3. According to the cooling effectiveness, ϕ, and heat transfer coefficient, h, they are calculated as the following equations, respectively.

Cooling effectiveness (ϕ):

$$\phi = \frac{T_\infty - T_{vane}}{T_\infty - T_{c,i}} \tag{1}$$

Heat transfer coefficient (h):

$$h = \frac{q_{flux}}{T_\infty - T_{wall}} \tag{2}$$

where T_∞ is the mainstream temperature, $T_{c,i}$ represents the coolant inlet temperature, and T_{vane} denotes the vane temperature. It should be noted that T_{vane} is replaced with the vane surface temperature, T_{wall}, and the vane volume temperature, T_{vol}, for the surface and volume bases, respectively. According to these bases, T_{wall} is the area-averaged vane surface temperature and T_{vol} which is the volume-averaged vane temperature is used for study on the sensitivity of volume cooling effectiveness in Section 4.3. According to the definition of h, T_∞ is used as the temperature reference and q_{flux} is heat flux transferring on the hot-side wall. A positive h shows that heat transfers from the fluid domain to the solid domain. Oppositely, if heat transfers from the solid domain to the fluid domain, h gives a negative value. As per the definition of ϕ expressed in equation (1), ϕ can be calculated using actual $T_{c,i}$ or the base $T_{c,i}$ of 339 K. The current study characterizes ϕ obtained by the actual and base coolant inlet temperatures.

4.1. Surface temperature

Fig. 2(a) presents surface temperature distributions at the vane midspan when $\Delta T_{c,i}$ increases from 0 to 8%. Undoubtedly, the increment in $T_{c,i}$ increases the surface temperature uniformly. Therefore, the trend of the surface temperature distributions obtained by increasing $T_{c,i}$ is the same as the base $T_{c,i}$ of 339 K, $\Delta T_{c,i}$ = 0%, does. Fig. 2(b) shows PS and SS contours of the surface temperature at different coolant inlet temperatures. Clearly, the contours also indicate that the surface temperature rises with increasing $T_{c,i}$. This phenomenon is explained by the fact that the temperature of the cooling air providing the film protection directly increases with $T_{c,i}$, thereby escalating the surface temperature significantly. Additionally, the results reflect on the significant influence of thermal conduction within the vane structure as $T_{c,i}$ from the cold-side source increases, as seen in Fig. 2(c). An interesting point observed from the results is that the vane temperature in a region of film holes R7-R9 where is near the stagnation on the PS is relatively high when compared to other regions affected by film cooling. This may happen due to high local static pressure in that region, as seen in Fig. 3(a) and relatively low cooling air from the film hole R8, as observed in Fig. 3(b). The phenomenon in such region is not disturbed by increasing $T_{c,i}$ because $T_{c,i}$ does not have a direct impact on flow fields of the mainstream and cooling air.

4.2. Surface cooling effectiveness

According to the definition of ϕ from equation (1), when the surface basis is employed, T_{vane} is replaced with T_{wall}. Basically, ϕ is a function of T_∞, T_{wall} and $T_{c,i}$. However, T_∞ is constant for the present study. Therefore, the variation of T_{wall} and $T_{c,i}$ results in ϕ only. Due to the aim of the present study, ϕ is presented in two aspects based on $T_{c,i}$ i.e. (1) actual and (2) base values. With the actual $T_{c,i}$, ϕ is computed using $T_{c,i}$ = 345.78, 352.56, 359.34 and 366.12 K for 2, 4, 6, and 8% rises, respectively. For the base $T_{c,i}$, the default

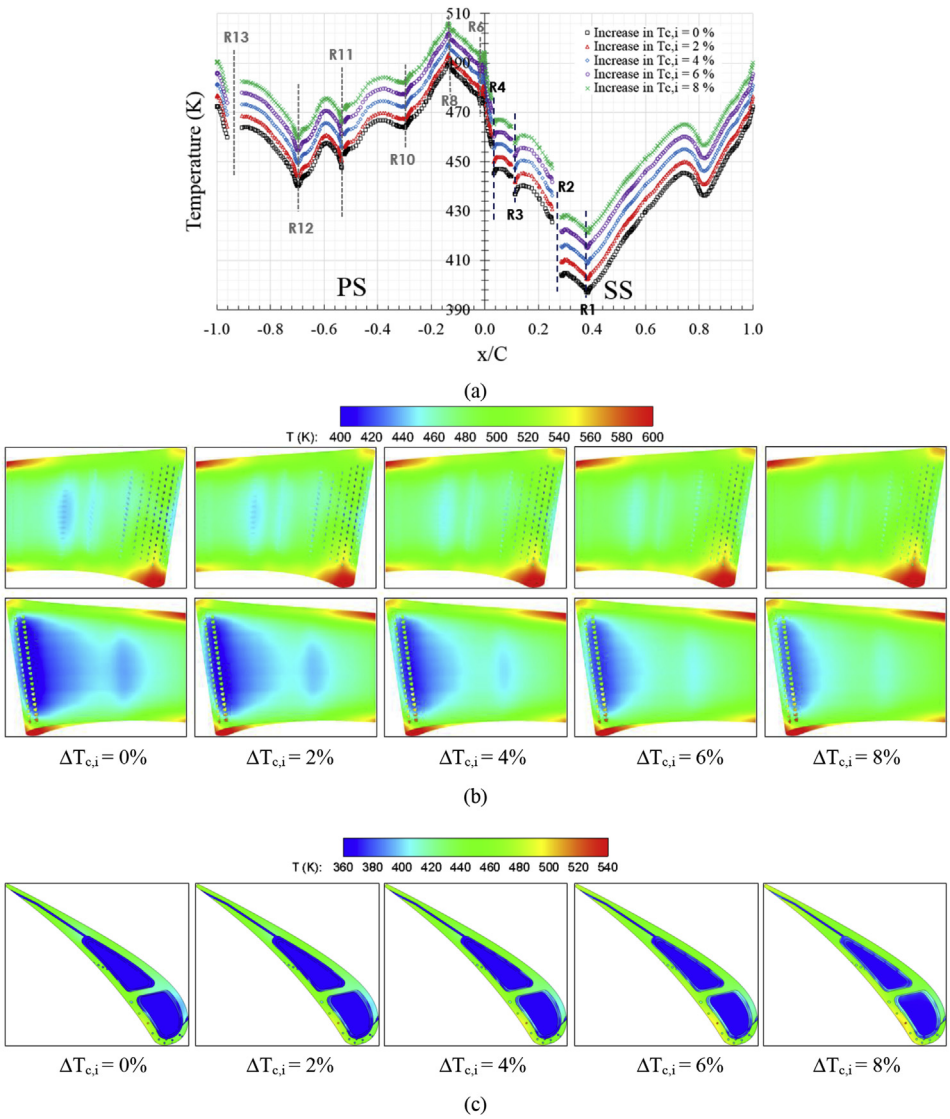

Fig. 2. Temperature distributions (a) along vane surface at midspan, (b) on PS and SS, (c) within vane body at midspan at different coolant inlet temperatures.

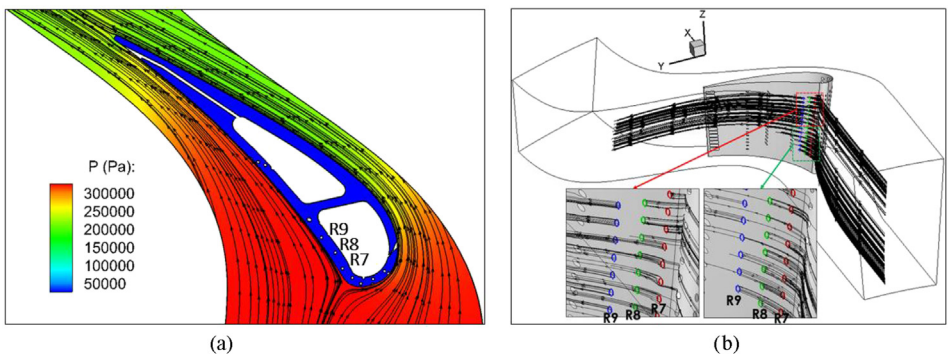

Fig. 3. Streamlines of (a) mainstream at midspan and (b) cooling air emitted from film holes R7-R9 at $\Delta T_{c,i}$ = 0%.

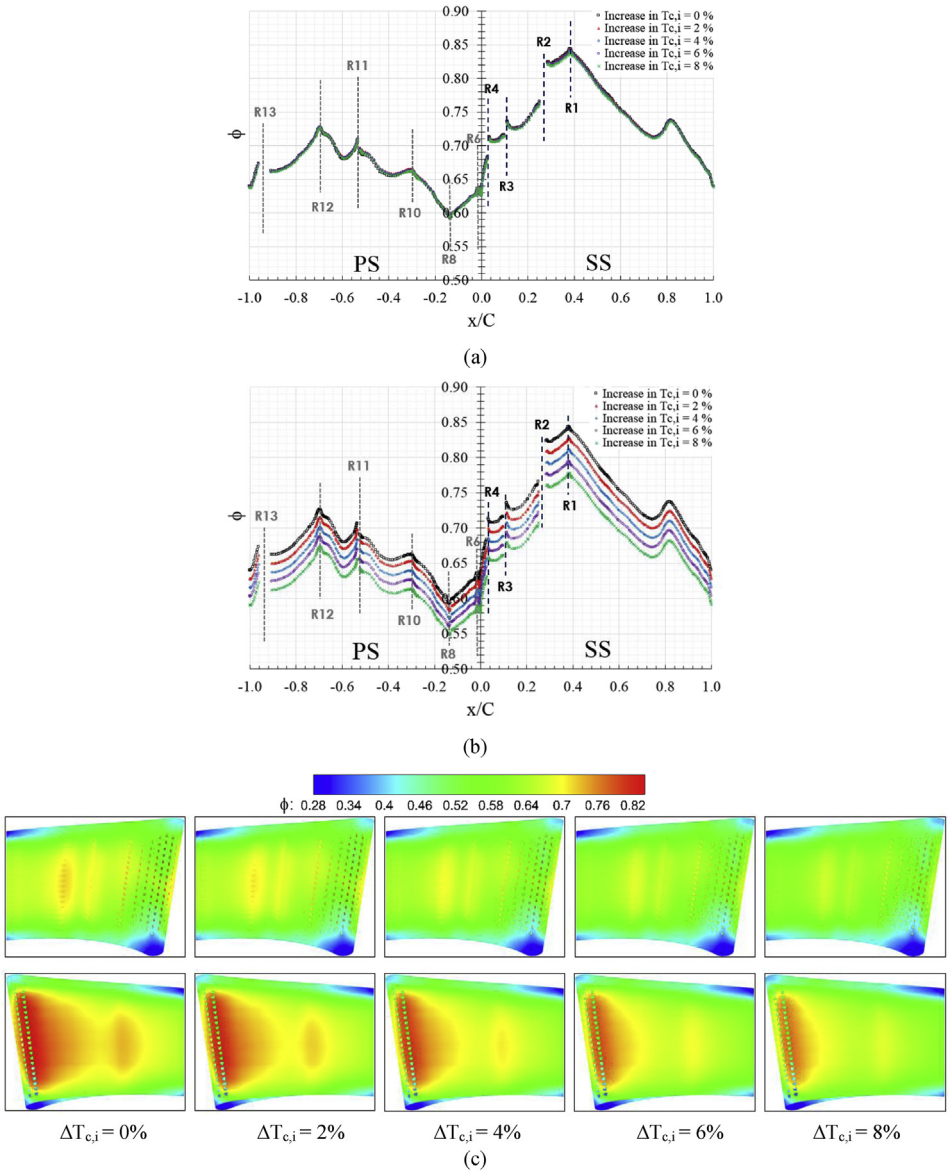

Fig. 4. Cooling effectiveness distributions (a) at midspan at different coolant inlet temperatures based on actual $T_{c,i}$, (b) base on $T_{c,i}$ = 339 K, and (c) on PS and SS at different coolant inlet temperatures based on $T_{c,i}$ = 339 K.

value of $T_{c,i}$ = 339 K is used to calculate ϕ. These two aspects of ϕ are characterized and discussed in this section. For the first aspect, distributions of ϕ obtained by the actual $T_{c,i}$ within the investigated range of 8% $T_{c,i}$ rise are presented in Fig. 4(a). The results show the slight variations of ϕ though $T_{c,i}$ rises to the maximum range. This may be explained by the fact that the temperature of cooling air emitted from film holes increases with the increment of $T_{c,i}$. Then, heat transfer driven by temperature differences on the hot-side wall decreases and T_{wall} increases. Hence, the variation of the $\frac{T_\infty - T_{wall}}{T_\infty - T_{c,i}}$ ratios with $T_{c,i}$ is slight. However, the variation of these distributions is different from that obtained by the second aspect. Based on the calculation using the base value, the default $T_{c,i}$ of 339 K is used for ϕ evaluation in equation (1) instead. Clearly, when $T_{c,i}$ increases, ϕ reduces uniformly, as seen in Fig. 4(b), and the variation trend of the distributions of ϕ corresponds to that of the temperature distributions shown in Fig. 2(a). This is reasonable because T_{wall} increases with $T_{c,i}$ as explained previously, whereas the difference between T_∞ and $T_{c,i}$ keeps constant. In addition, Fig. 4(c) shows PS and SS contours of ϕ obtained by $T_{c,i}$ = 339 K at different coolant inlet temperatures. Obviously, when the base $T_{c,i}$ is used, the PS and SS contours show the visible variation of ϕ when $T_{c,i}$ increases. The increment in $T_{c,i}$ decreases ϕ drastically, especially on the SS. These phenomena suggest that although ϕ obtained by using the actual $T_{c,i}$ is quite straightforward and follows the definition directly, ϕ obtained by using the base $T_{c,i}$ is more understandable because it corresponds to the variation of the surface temperature when $T_{c,i}$ changes. The results obtained from both aspects are characterized that if the actual $T_{c,i}$ is used, T_∞ - $T_{c,i}$ decreases and ϕ changes slightly, whereas T_∞ - $T_{c,i}$ keeps unchanged if the base $T_{c,i}$ is chosen, thereby reducing ϕ drastically. The

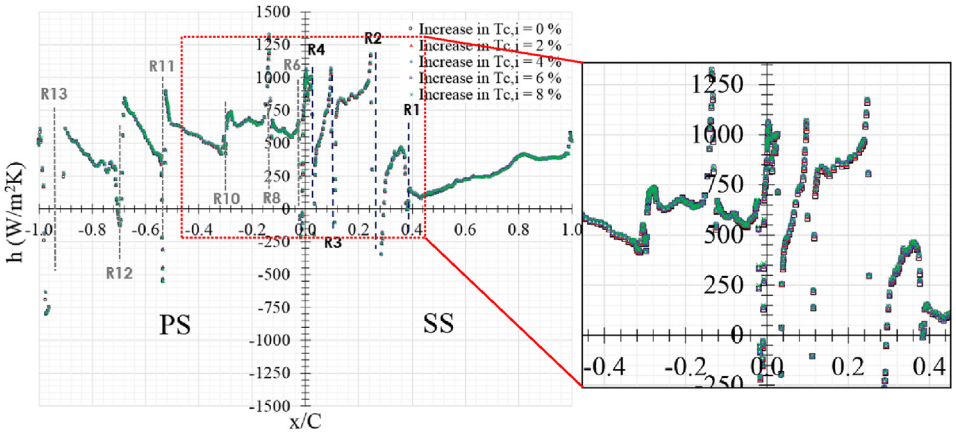

Fig. 5. Heat transfer coefficient distributions at midspan at different coolant inlet temperatures.

results also show that the variation of heat transfer coefficient distributions obtained by equation (2) is quite slight though $T_{c,i}$ increases to the maximum value, as seen in Fig. 5. In addition, considering the surface basis, equations (1) and (2) can get re-arrangement as below:

$$\phi = \frac{T_\infty - T_{wall}}{T_\infty - T_{c,i}} \tag{3}$$

$$T_\infty - T_{wall} = \phi(T_\infty - T_{c,i}) \tag{4}$$

Inserting equation (4) in equation (2), therefore:

$$h = \frac{q_{flux}}{T_\infty - T_{wall}} = \frac{q_{flux}}{\phi(T_\infty - T_{c,i})} \tag{5}$$

Equation (5) indicates that even though T_{wall} depends on $T_{c,i}$, the change of h is slight with $T_{c,i}$ - no matter that either the actual or base $T_{c,i}$ is used for h calculation. This result is completely different from the ϕ calculation. Following these phenomena, equation (5) suggests that the amount of heat flux on the hot-side wall needs to be decreased for both aspects. PS and SS contours of the surface heat flux confirm this suggestion, as seen in Fig. 6(a) and (b), respectively. Evidently, the contours indicate the reduction of heat flux at higher coolant inlet temperatures, especially in regions where are marked with A, B, and C.

4.3. Sensitivity of volume cooling effectiveness and temperature

It is well-known that the cooling air is taken from the compressor discharge, and directed to the turbine vane to provide efficiently adequate cooling to maintain the metal temperature of the vane below the maximum allowable temperature. When the coolant flows through supply passages till the exit of film holes, its temperature increases as its pressure reduces. Hence, the effects of the increase in $T_{c,i}$ supplied by the compressor on the sensitivity of ϕ of the vane are investigated based on the volume basis – T_{vol} is used in equation (1) for the ϕ evaluation. Fig. 7 presents variations of the volume vane temperatures and ϕ based on the actual and base values of $T_{c,i}$ as $T_{c,i}$ increases in the investigated range of 0–8%. Among these variations, it is clear that ϕ_{base} and temperature vary linearly and sensitively, but ϕ_{actual} varies slightly and seems insensitively with the increment of $T_{c,i}$. This indicates the downside of using the actual $T_{c,i}$ for the sensitivity of ϕ due to the ratio of $\frac{T_\infty - T_{vol}}{T_\infty - T_{c,i}}$ changes slightly like in the previous discussion in Section 4.2. Hence, the base $T_{c,i}$ of 339 K is used for the following discussion. Obviously, the results indicate that an 8% rise in $T_{c,i}$ causes 18 K and 25 K increments in the T_{av} and T_{min}, respectively, thereby reducing ϕ_{av} and ϕ_{max} significantly from 0.665 to 0.616 and 0.869 to 0.802, respectively. These phenomena are reasonable because ϕ_{max} is directly linked to T_{min}, which should exist in the cold-side wall. Therefore, when $T_{c,i}$ increases, T_{min} increases directly and results in the dramatic reduction of ϕ_{max}. Moreover, this dramatic reduction also leads to the significant reduction of ϕ_{av} because the variation of ϕ_{av} depends upon the variation of the vane metal temperature from the hot-side wall to the cold-side wall. This driving temperature is directly linked to the temperature difference between hot and cold sources. When $T_{c,i}$ increases, the driving temperature decreases. As a result, ϕ_{av} is reduced in the circumstances. Another observation is that the reduction of ϕ_{min} (from 0.266 to 0.247) is lower than that of ϕ_{av} and ϕ_{max} within the investigated range, and only increasing 7 K in T_{max} from the 8% rise in $T_{c,i}$. This may be explained by the fact that ϕ_{min} is related to T_{max} which exists in the hot-side wall, especially in regions where are cooled ineffectively by cooling air. The increment in $T_{c,i}$ affects T_{max} indirectly because it exists on the hot-side wall. As a result, the change in T_{max} is small. As seen previously in Fig. 5, the increase in $T_{c,i}$ has a slight effect on the heat transfer coefficient. Consequently, the increase in T_{max} is lower than that in T_{av} and T_{min}.

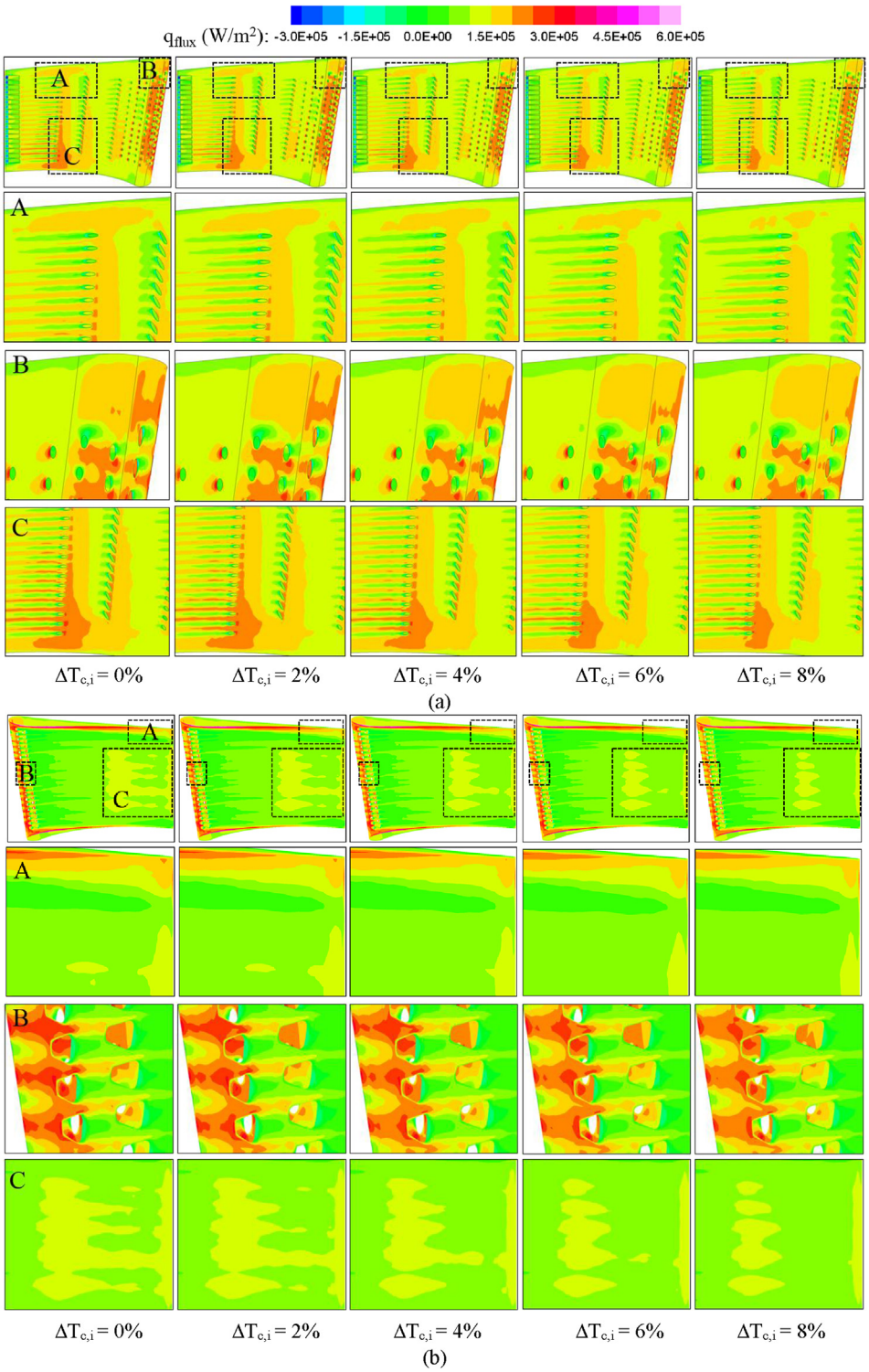

Fig. 6. Surface heat flux distributions on (a) PS and (b) SS at different coolant inlet temperatures.

5. Conclusion

This work presents a case study of cooling effectiveness, which is used for cooling performance discussion of turbine airfoils, under the effects of coolant inlet temperature in two aspects based on the actual and base coolant inlet temperature calculations. The

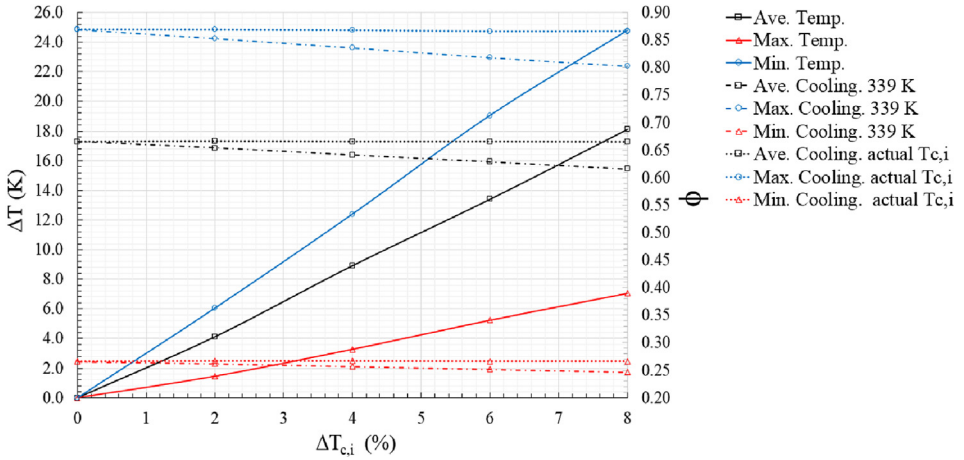

Fig. 7. Sensitivity of cooling effectiveness and vane temperatures.

film-cooled vane and the annular cascade flow of the mainstream are simulated to conduct the heat transfer parameters in terms of temperature, cooling effectiveness, and heat transfer coefficient using CFD/CHT analysis. The sensitivity of the vane temperature and cooling effectiveness under the effect of coolant inlet temperature is discussed also. Results show that for the surface basis, although the cooling effectiveness obtained by using the actual coolant inlet temperature is quite straightforward and follows the definition of the cooling effectiveness directly, the cooling effectiveness obtained by using the base coolant inlet temperature is more understandable because it corresponds to the variation of the surface temperature when coolant inlet temperature changes. The results obtained by the surface basis is expanded to the volume basis for the cooling sensitivity. Based on the base coolant inlet temperature, the 8% increase in the coolant inlet temperature results in the reduction of the average cooling effectiveness from 0.665 to 0.616 and the maximum cooling effectiveness from 0.869 to 0.802. These correspond to 18 K and 25 K increments in the vane average and minimum temperatures, respectively. In addition, the reduction of the minimum cooling effectiveness is lower than that of the average and maximum cooling effectiveness. This shows only 7 K increase in the maximum temperature at 8% rise in the coolant inlet temperature. However, when the actual coolant inlet temperature is used, the results show insensitive cooling effectiveness due to the reduction of heat flux on the hot-side wall as the coolant inlet temperature increase. It is expected that the results and phenomena obtained here are different from those obtained by changing other variables such as the mainstream inlet temperature, pressure ratio, and blowing ratio.

Acknowledgements

This research is supported by The National Key Research and Development Program of China (2017YFB0202802) and National Natural Science Foundation of China (11702297). The first author would like to express appreciation to the Chinese Academy of Sciences (CAS) for giving an opportunity to do research under the PIFI programme at the Institute of Mechanics. In addition, the first author would like to express gratitude to Professor Jianhua Wang, Dr. Huazhao Xu, and Mr. Qingbo Zhang, University of Science and Technology of China for their support. Lastly, the first author is grateful for the full support of King Mongkut's Institute of Technology Ladkrabang.

References

[1] L. Mangani, M. Cerutti, M. Maritano, M. Spel, Conjugate Heat Transfer Analysis of NASA C3X Film Cooled Vane with an Object-Oriented CFD Code, (2010) ASME Paper No. GT2010-23458.
[2] Z.Q. Ke, J.H. Wang, Conjugate heat transfer simulations of pulsed film cooling on an entire turbine vane, Appl. Therm. Eng. 109 (2016) 600–609.
[3] R.H. Ni, W. Humber, G. Fan, P.D. Johnson, J. Downs, J.P. Clark, J.P. Koch, Conjugate Heat Transfer Analysis of a Film-Cooled Turbine Vane, (2011) ASME Paper No. GT2011-45920.
[4] W.D. York, J.H. Leylek, Three-Dimensional Conjugate Heat Transfer Simulation of an Internally-Cooled Gas Turbine Vane, (2003) ASME Paper No. GT2003-38551.
[5] M.R. Reyhani, M. Alizadeh, A. Alireza Fathi, H. Khaledi, Turbine blade temperature calculation and life estimation - a sensitivity analysis, Propul. Power Res. 2 (2) (2013) 148–161.
[6] M. Alizadeh, A. Izadi, A. Fathi, Sensitivity analysis on turbine blade temperature distribution using conjugate heat transfer simulation, J. Turbomach. 136 (2014) 011001.
[7] J.H. Liu, Y.B. Liu, L. Liu, Film cooling modeling of a turbine vane with multiple configurations of holes, Case Stud. Therm. Eng. 11 (2018) 71–80.
[8] B.S. Kim, B.S. Kim, W.S. Choi, G.O. Musgrove, J. McFarland, F. Fierro, D.L. Ransom, Gas Turbine Blade Stress and Temperature Sensitivity to Turbine Inlet Profile and Cooling Flow, (2012) ASME Paper No. GT2012-69603.
[9] R.P. Williams, T.E. Dyson, D.G. Bogard, S.D. Bradshaw, Sensitivity of the overall effectiveness to film cooling and internal cooling on a turbine vane suction side, J. Turbomach. 136 (2014) 031006.
[10] F. Espinosa, A. Portugal, D. Narzary, F. Cadena, J. Han, J. Kubiak, S. Blake, H. Lara, Influence of Cooling Flow Rate Variation on Gas Turbine Blade Temperature Distributions, (2008) ASME Paper No. GT2008-50103.
[11] T. Roos, “NGV Trailing Edge Ejection Slot Size Sensitivity Study,” Paper No. ISABE-2005-1158, (2005).

[12] M.L. Nathan, T.E. Dyson, D.G. Bogard, S.D. Bradshaw, Adiabatic and overall effectiveness for the showerhead film cooling of a turbine vane, J. Turbomach. 136 (2014) 031005.
[13] E.E. Halila, D.T. Lenahan, T.T. Thomas, "Energy Efficient Engine High Pressure Turbine Test Hardware Detailed Design Report," NASA CR-167955, NASA Lewis Research Center, 1982.
[14] Q.B. Zhang, H.Z. Xu, J.H. Wang, G. Li, L. Wang, X.Y. Wu, S.Y. Ma, "Evaluation of CFD Predictions Using Different Turbulence Models on a Film Cooled Guide Vane under Experimental Conditions," ASME Paper No. GT2015-42563, (2015).
[15] J.H. Liu, Y.B. Liu, X. He, L. Liu, Study on TBCs insulation characteristics of a turbine blade under serving conditions, Case Stud. Therm. Eng. 8 (2016) 250–259.
[16] L.P. Timko, Energy Efficient Engine High Pressure Turbine Component Test Performance Report; NASA CR-168289, NASA Lewis Research Center, Cleveland, OH, USA, 1984.
[17] P. Prapamonthon, H.Z. Xu, W.S. Yang, J.H. Wang, Numerical study of the effects of thermal barrier coating and turbulence intensity on cooling performances of a nozzle guide vane, Energies 10 (3) (2017) 362.
[18] E. Lutum, F. Cottier, M.E. Crawford, B. Laveau, R.S. Abhar, A computational investigation of the effect of surface roughness on heat transfer on the stator endwall of an axial turbine, Proc. IMechE. Part A: J Power and Energy 229 (5) (2015) 454–464.
[19] Z.Q. Ke, J.H. Wang, Numerical investigations of pulsed film cooling on an entire turbine vane, Appl. Therm. Eng. 87 (5) (2015) 117–126.